ACS APPLIED NANO MATERIALS

www.acsanm.org Letter

Rhodium Oxide Nanorod Motors Powered by Light across the Full Visible Spectrum

Donghao Cui, Xianglong Lyu, Shifang Duan, Yixin Peng, and Wei Wang*

Cite This: https://doi.org/10.1021/acsanm.2c03560 Read Online

ACCESS | Metrics & More | Article Recommendations | Supporting Information

ABSTRACT: We report nanorod motors made of gold (Au) and rhodium oxide (Rh_2O_3) that move in UV and visible light (purple, blue, green, or red). These nanorods are synthesized in large quantities (10^9/batch) by template-assisted electrodeposition, followed by annealing, and are uniformly distributed and resist strong acids or bases. Rh_2O_3 forms a heterojunction with Au so that a Rh_2O_3–Au nanorod moves toward Au under visible light via self-electrophoresis. Its speed increases with light intensities and fuel [e.g., hydrogen peroxide (H_2O_2)] concentrations, reaching 28.5 μm/s in 10% H_2O_2 under 365 nm light of 320 mW/cm^2. These nanorod motors also form dynamic and reversible clusters under light.

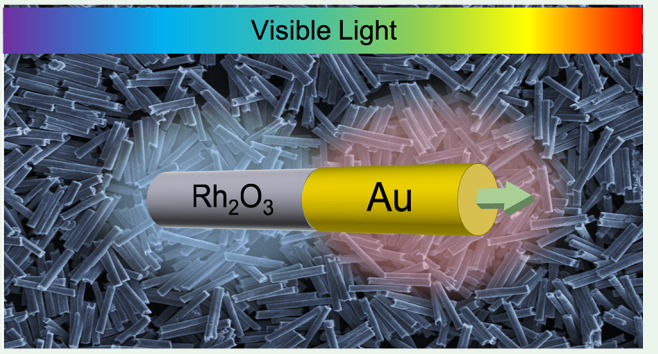

KEYWORDS: *micro/nanomotor, electrodeposition, rhodium oxide, photocatalysis, large-scale synthesis*

Micro/nanomotors that convert energy stored in the environment into motion at small scales have attracted much attention in the past 20 years.[1−3] Among the various types of energy sources, light is particularly attractive because of its tunability in intensity,[4−11] polarization,[12] incident direction,[13] spatiotemporal distribution,[14] and wavelength,[4,5,8,10,15−17] which allows for control of the speed and direction of a nanomotor with high degrees of freedom.

The ability for a micro/nanomotor to respond to the entire spectrum of visible light[5−7,9−11] could open up even more opportunities that not only enable new applications but also facilitate the studies of active matter.[18] Despite the recent progress of micro/nanomotors that move under visible light, such as $BiVO_4$,[19] Cu_2O–Au,[17] Fe_2O_3–Au,[16] C_3N_4,[15] B–TiO_2,[4] etc., only a few can move in the entire spectrum of visible light (400−700 nm). Examples include dye-sensitized nanotree swimmers,[10] $Zn_xCd_{1-x}Se$ alloy nanowire motors,[7] and bubble-propelled tubular micromotors functionalized with quantum dots.[9] There is a continuous need for the development of new light-driven micro/nanomotors that move under the full spectrum of visible light, preferably in large quantities to reduce cost and enable studies of their collective behaviors.[20,21]

Here, we report nanorods made of rhodium oxide (Rh_2O_3) and gold (Au) that autonomously move toward the Au side in aqueous solutions of hydrogen peroxide (H_2O_2) under illumination of light from UV through the full visible spectrum. Its speed can be easily tuned by adjusting the H_2O_2 concentration, the intensity, or the wavelength of incident light. These Rh_2O_3–Au nanorods can be synthesized uniformly in large quantities (10^9/batch) by template-assisted electrochemical deposition, making it a good model system for studying their collective behaviors.[22,23] As an example, we showcase at the end the reversible assembly of a dense population of these rods into dynamic clusters. These Au–Rh_2O_3 motors swim at ∼1 body length/s in 0.1% H_2O_2 under 80 mW/cm^2 and are therefore potentially useful for environmental sensing and remediation under sunlight.

Rh_2O_3–Au nanorods were prepared by annealing Rh–Au nanorods in air (shown in Figure 1a). First, Rh–Au bimetallic nanorods of ∼310 nm diameter and ∼2.6 μm length were first electrodeposited in a commercially available aluminum oxide (AAO) template. Then, the nanorod-filled template was annealed in an air-filled furnace to oxidize Rh into Rh_2O_3, typically at 700 °C for 4 h (this is the optimum annealing condition chosen from a range of conditions listed in Table S1). The AAO template was then dissolved in sodium hydroxide (NaOH), yielding roughly 2 billion (2×10^9) Rh_2O_3–Au nanorods from one commercial AAO membrane of 25 mm diameter. More experimental details are given in the Supporting Information (SI).

Representative images of these rods under a scanning electron microscope are given in Figure 1b. These samples were highly uniform in size, with the polydispersity index (PDI) being ∼0.01 for rod diameters of 307 ± 34 nm and

Received: August 11, 2022
Accepted: October 13, 2022

ACS Publications © XXXX American Chemical Society

https://doi.org/10.1021/acsanm.2c03560
ACS Appl. Nano Mater. XXXX, XXX, XXX−XXX

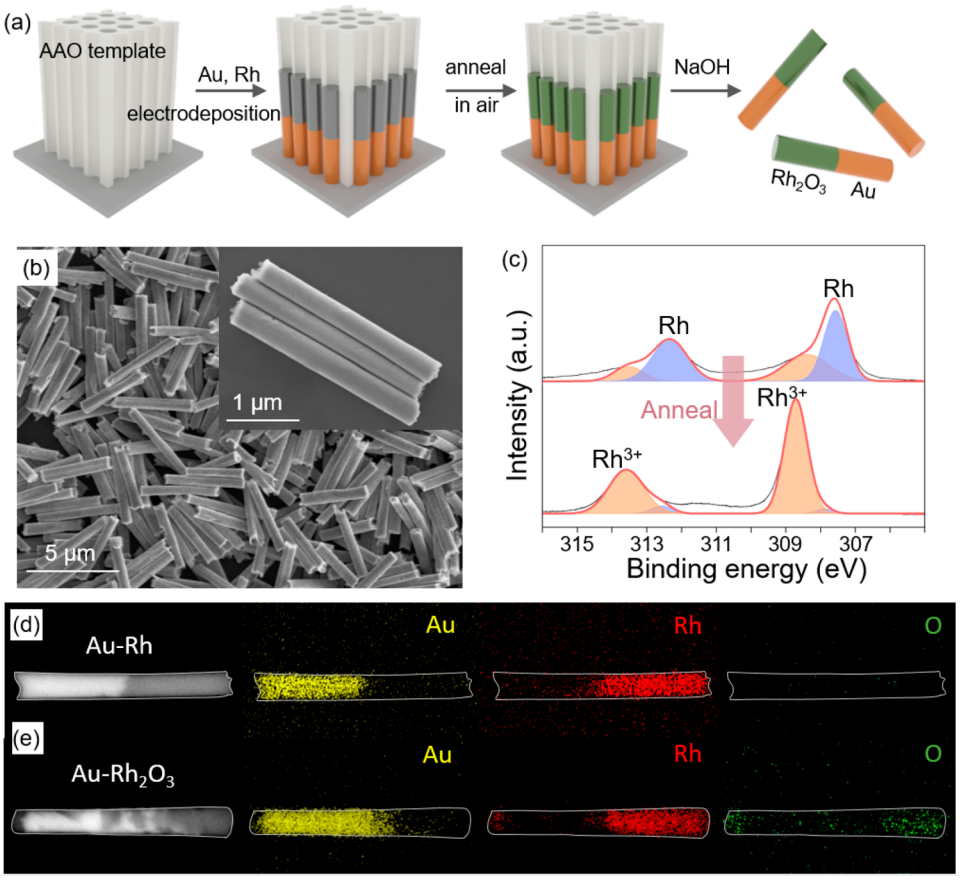

Figure 1. Preparation and characterization of Rh_2O_3–Au nanorod motors. (a) Synthesis of Rh_2O_3–Au nanorods by electrodeposition in an AAO template, followed by annealing in a furnace. See the main text and SI for details. (b) SEM images of Rh_2O_3–Au rods. (c) XPS spectra suggesting conversion from Rh^0 to Rh^{3+} on the rod surface after annealing. (d and e) Backscattered SEM images and elemental mapping of Au, Rh, and O for a Rh–Au rod (d) and a Rh_2O_3–Au rod (e).

~0.02 for rod lengths of 2.59 ± 0.32 μm (see Figure S1 for size distributions; PDI is defined as the square of the standard deviation divided by the mean value[24]). The small but nonnegligible sample polydispersity was caused either by the intrinsic nonuniformity of the membrane or by the electrodeposition process. X-ray photoelectron spectroscopy (XPS; Figure 1c) and scanning electron microscopy–elemental mapping (SEM–EDS; Figure 1d,e) confirmed the successful conversion of Rh to Rh_2O_3 after annealing and that Rh_2O_3 and Au were mainly located at either end of the bisegmented rod. A similar conversion from Rh to Rh_2O_3 by thermal annealing was reported in ref 25 although not for nanorods.

A few comments are worth noting regarding the synthesis of a Rh_2O_3–Au nanorod. First, nanorods of different lengths can be made by varying the deposition conditions, and nanorods of metal segments other than Au can be synthesized by replacing the plating solutions. Second, Au and Rh tend to diffuse into each other during annealing (see Figure 1e for an example). Such a diffusion could lead to rods of more erratic distributions of Au and Rh_2O_3 and could contribute to the circular motion of the Rh_2O_3–Au nanomotors in H_2O_2. A complete understanding of how the material diffusion affects the resulting motion is, however, lacking at the moment. Finally, annealing at high temperatures and for long duration often causes severe deformation of the rods (see Figure S1 for an example), while annealing at low temperatures and for shorter duration might not fully oxidize the rods. The latter issue could, in principle, be resolved by increasing the partial pressure of oxygen based on simple thermodynamic reasoning. A wide range of synthesis conditions have been tested, and the results are listed in Table S1.

Rh_2O_3–Au rods moved toward the Au end in a H_2O_2 solution when illuminated by light but only showed Brownian motion without light (Figure 2a). As a result, their propulsion can be switched on or off with light (Figure 2b). They often moved in spiral or circular trajectories, possibly because of the diffusion of metal segments during annealing described above or the intrinsic shape asymmetry of rods from the nonuniformity of the template. Most notably, Rh_2O_3–Au nanorods were able to move in light across the full visible spectrum, but they moved more slowly as the wavelength shifted to red. Examples of their propulsion in purple, blue, green, and red light are shown in Figure 2c–f (note that they moved even faster in UV light, but this result is expected and therefore not shown here; moreover, red light beyond 660 nm was not tested in order to minimize the photothermal effect of Au, which could complicate a rod's propulsion). In addition, they moved faster in higher concentrations of H_2O_2 and higher light intensity (Figure 2g,h), consistent with typical photocatalytic micro/nanomotors reported in the literature.[4,9,16,17] As a result, their speeds can be precisely tuned by a combination of these experimental parameters. As a special case, these Au–Rh_2O_3 motors swim at 2.2 μm/s in 0.1% H_2O_2 under 80 mW/cm^2, a reasonable condition for processing

https://doi.org/10.1021/acsanm.2c03560
ACS Appl. Nano Mater. XXXX, XXX, XXX–XXX

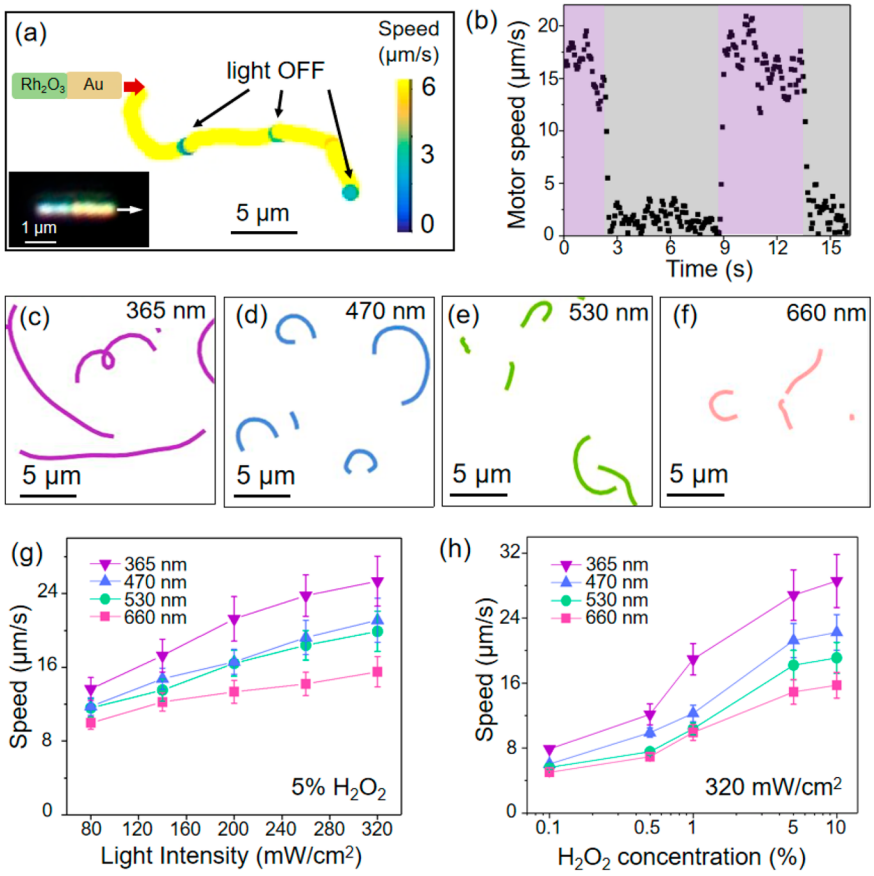

Figure 2. Motion of Rh_2O_3–Au nanorod motors. (a) Trajectory of a Rh_2O_3–Au nanorod over 6 s in 5% H_2O_2 under 470 nm light (taken from Video S1). Light was turned off at three labeled instances. The trajectory is color-coded with the instantaneous speed of the motor. Inset: Rh_2O_3–Au nanorod moving toward the Au end, as seen under dark-field microscopy (taken from Video S2). (b) Instantaneous speeds of a Rh_2O_3–Au nanorod when 470 nm light was switched on and off. (c–f) Trajectory of Rh_2O_3–Au nanorods over 2 s in 5% H_2O_2 under light of 365, 470, 530, and 660 nm, respectively (taken from Video S3). Average speeds of Rh_2O_3–Au nanomotors under different wavelengths of light (g) and in different concentrations of H_2O_2 (h). The error bars in parts g and h are standard deviations of ~50 measurements. The data in parts g and h are from Video S4.

wastewater under sun light, suggesting potential applications in environmental remediation.

We propose that a Rh_2O_3–Au nanorod contains a heterojunction that enables photocatalysis, which moves the rod via self-electrophoresis. To elaborate, Rh_2O_3 is a p-type semiconductor with a band gap of ~1.41 eV,[26] corresponding to a maximum absorption wavelength of up to ~880 nm. Rh_2O_3 then forms a Schottky junction with Au so that, when illuminated by light, electrons and holes are excited in Rh_2O_3 and preferably transported to the Rh_2O_3–water and Au–water interfaces, respectively, where the reduction and oxidation half-reaction of H_2O_2 occurs (see Figure 3a for the schematic). As a result, a proton gradient is generated around the nanorod pointing from the Au end to the Rh_2O_3 end, and the negatively charged nanorod (ζ potential of −46 mV) moves in this self-generated electric field and toward Au. This mechanism, known as self-electrophoresis,[27] is widely believed to be responsible for the autonomous motion of the classic bimetallic nanorods in H_2O_2,[28] as well as many other photocatalytic nanomotors consisting of a metal–semiconductor heterojunction.[4,6,8,16,17,20]

Self-electrophoresis of a Rh_2O_3–Au nanorod undergoing photocatalysis is supported by photocurrent measurements. First, as shown in Figure 3b,c, photogenerated electrons flow from a Au electrode to a Rh_2O_3 electrode immersed in aqueous H_2O_2 solutions when illuminated by light. The presence of such a photocurrent between Rh_2O_3 and Au and its direction are consistent with the proposed mechanism. Second, parts d–g of Figure 3 show that the changes in the photocurrents match those in the motor speeds when the light intensities and wavelengths were varied. This provides strong evidence that the motor speeds are directly related to the photocurrents, which dictate the ion fluxes in and out of a Rh_2O_3–Au nanorod and ultimately the strength of the self-generated electric field.

One advantage of Rh_2O_3–Au nanomotors synthesized by electrodeposition is their large quantities, which enables the study of collective behaviors in population densities (φ, defined as 2D coverage) as high as 75%. Experiments of such high population densities are difficult for other photocatalytic nanomotors, such as those made of silicon nanowires[11] or by asymmetrically coating TiO_2 microspheres,[20] mostly because of the limited amount of sample. No significant bubble was observed even at very concentrated suspensions possibly because Rh_2O_3 is not as catalytically active toward the decomposition of H_2O_2 as Rh is. This lack of large bubbles is yet another key advantage over conventional bimetallic nanorod motors because it permits experiments of large population densities, as we demonstrated in this paper.

https://doi.org/10.1021/acsanm.2c03560
ACS Appl. Nano Mater. XXXX, XXX, XXX−XXX

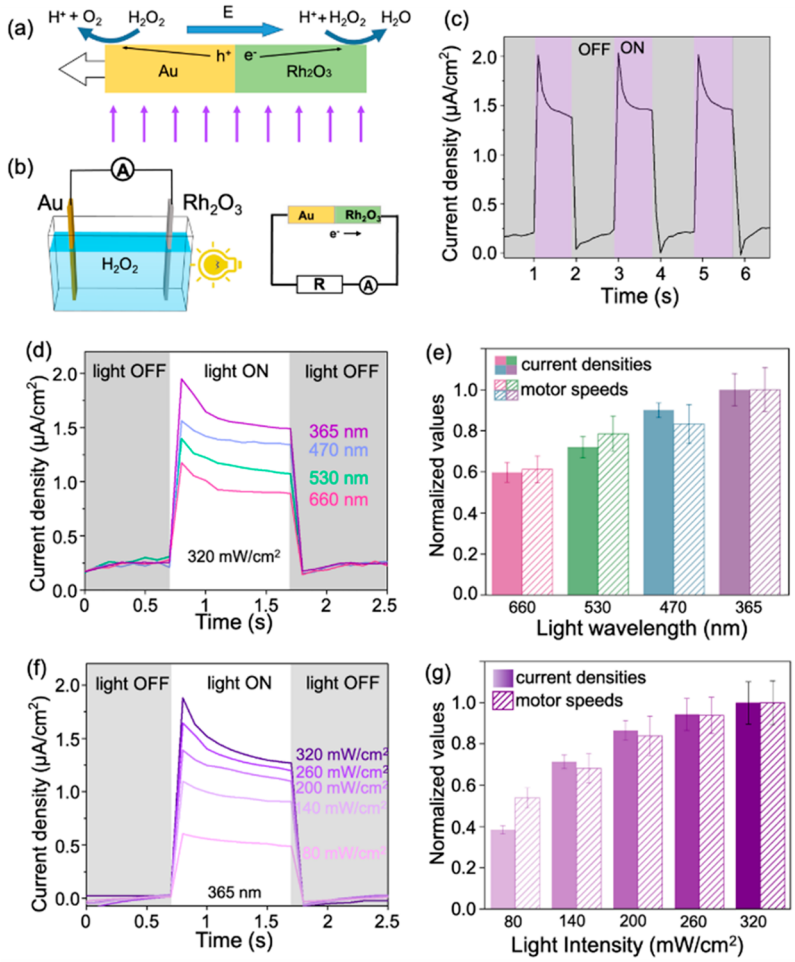

Figure 3. Propulsion mechanism of Rh_2O_3–Au nanomotors. (a) Schematic of self-electrophoresis of a Rh_2O_3–Au nanorod in H_2O_2. See the main text for detailed descriptions. (b) Schematic of the electrochemical setup to measure the photocurrent between Au and Rh_2O_3 electrodes and an equivalent circuit. Positive photocurrent values correspond to electrons flowing from Au to Rh_2O_3. (c) Instantaneous photocurrents measured with the setup shown as part b in 5% H_2O_2 under 365 nm light of 320 mW/cm^2. (d) Photocurrent densities in 5% H_2O_2 under light of different wavelengths, with the same light intensity of 320 mW/cm^2. These results are normalized and compared in part e with motor speeds obtained under the same lighting conditions (speed data obtained from Figure 2g). (f and g) Photocurrent densities and motor speeds at different light intensities in 5% H_2O_2 under 365 nm light. The error bars of the current densities in parts e and g are standard deviations of photocurrent measurements during the entire period of illumination in parts d and f, respectively. The error bars of the motor speeds are from Figure 2g.

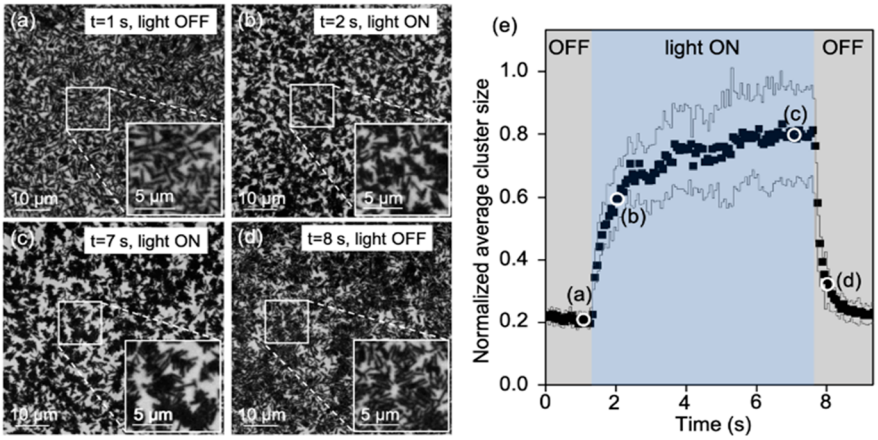

Figure 4. Dynamic clustering of Rh_2O_3–Au motors (snapshots taken from Video S5). (a) Rh_2O_3–Au rods of a 2D coverage φ = 67% were suspended in 5% H_2O_2. (b) Rods quickly formed moving clusters when irradiated with 470 nm light of 200 mW/cm^2. (c) Over a few seconds, clusters of Rh_2O_3–Au rods reached a steady-state size distribution. (d) Clusters disintegrated when light was switched off. (e) Normalized cluster size (defined as the number of rods in a cluster) measured over time, with the labeled time instances corresponding to parts a–d. The error bars are the standard deviations of all of the cluster sizes measured in one optical micrograph.

https://doi.org/10.1021/acsanm.2c03560
ACS Appl. Nano Mater. XXXX, XXX, XXX–XXX

As an example of the collective behaviors of Rh_2O_3–Au nanorods under light, Figure 4 and Video S5 show that Rh_2O_3–Au nanorods of φ = 67% quickly formed dynamic clusters in 5% H_2O_2 when irradiated by blue light (470 nm) for a few seconds. These dynamic clusters formed and broke continuously, and each cluster could rotate or move linearly depending on the exact arrangement of the rods within a cluster. Clusters dissolved when light was switched off. This dynamic process is quantified in Figure 4e by the rise and fall of the average cluster size. Experiments performed in other concentrations of H_2O_2 or light intensities/wavelengths were not qualitatively different from the example shown here, as long as rods were motile.

Finally, we note that another key advantage of Rh_2O_3–Au nanorods over nanorod motors made of Cu_2O[17] or iron oxides[16] is their chemical inertness toward strong acids or bases. For example, Figure S3 confirms that Rh_2O_3–Au nanorods remained structurally intact after soaking in 68% HNO_3 or 10 mol/L NaOH solutions overnight and were still motile in H_2O_2 afterward. Although acid/base resistant, Rh_2O_3–Au nanorods cannot move in strong acids or bases because self-electrophoresis fails at high ionic strengths, a well-known limitation to this particular driving mechanism.[29]

In conclusion, we have developed Rh_2O_3–Au nanorod motors that autonomously move in the full spectrum of visible light in H_2O_2 aqueous solution via self-electrophoresis. They are synthesized uniformly in large scale using template-assisted electrochemical deposition. Their speeds can be easily and precisely controlled by varying the fuel concentration, light intensity, and wavelength. A maximum speed of 28.5 μm/s was found in 10% H_2O_2 irradiated with 365 nm light of 320 mW/cm^2. Rh_2O_3–Au nanorod motors readily form dynamic, reversible clusters, at population densities as high as 67%. Rh_2O_3–Au nanorod motors reported here could be used for environmental remediation, microassembly, or cargo delivery under visible light. They are also a good model system for studying rod-shaped active matter,[22,30] particularly at high population densities.

■ ASSOCIATED CONTENT

Supporting Information

The Supporting Information is available free of charge at https://pubs.acs.org/doi/10.1021/acsanm.2c03560.

Synthesis of micromotors, supporting data including the preparation details, size distribution, annealing condition, and inertness against strong acid and base, the motor experiment, and electrochemical measurements (PDF)

Au–Rh_2O_3 nanomotors activated or stopped by switching the lamp on and off (motors in 5% H_2O_2 under 470 nm light of 200 mW/cm^2) (MP4)

Observing the moving direction of Au–Rh_2O_3 nanomotors in the dark field [3× speed; motor in 5% H_2O_2 under a mercury lamp of ~50 mW/cm^2; this video was taken with an upright microscope (Olympus BX51M) in the reflective mode] (MP4)

Au–Rh_2O_3 nanomotors moving under the illumination of different wavelengths (motors in 5% H_2O_2 under 365, 470, 530, and 660 nm light of 200 mW/cm^2) (MP4)

Au–Rh_2O_3 nanomotors moving under different illumination intensities and in different concentrations of H_2O_2 (motors under 365, 470, 530, and 660 nm light) (MP4)

Collective behaviors of Au–Rh_2O_3 nanomotors (motors in 5% H_2O_2 under 470 nm light of 200 mW/cm^2) (MP4)

■ AUTHOR INFORMATION

Corresponding Author

Wei Wang – *School of Materials Science and Engineering, Harbin Institute of Technology (Shenzhen), Shenzhen, Guangdong 518055, China*; orcid.org/0000-0003-4163-3173; Email: weiwangsz@hit.edu.cn

Authors

Donghao Cui – *School of Materials Science and Engineering, Harbin Institute of Technology (Shenzhen), Shenzhen, Guangdong 518055, China*

Xianglong Lyu – *School of Materials Science and Engineering, Harbin Institute of Technology (Shenzhen), Shenzhen, Guangdong 518055, China*

Shifang Duan – *School of Materials Science and Engineering, Harbin Institute of Technology (Shenzhen), Shenzhen, Guangdong 518055, China*

Yixin Peng – *School of Materials Science and Engineering, Harbin Institute of Technology (Shenzhen), Shenzhen, Guangdong 518055, China*

Complete contact information is available at: https://pubs.acs.org/10.1021/acsanm.2c03560

Notes

The authors declare no competing financial interest.

■ ACKNOWLEDGMENTS

This project is financially supported by the Shenzhen Science and Technology Program (Grants JCYJ20190806144807401, JCYJ20210324121408022, and RCYX20210609103122038).

■ REFERENCES

(1) Chen, X.; Zhou, C.; Wang, W. Colloidal Motors 101: A Beginner's Guide to Colloidal Motor Research. *Chem. Asian J.* **2019**, *14* (14), 2388–2405.

(2) Mallouk, T. E.; Sen, A. Powering Nanorobots. *Sci. Am.* **2009**, *300* (5), 72–77.

(3) Medina-Sánchez, M.; Magdanz, V.; Guix, M.; Fomin, V. M.; Schmidt, O. G. Swimming Microrobots: Soft, Reconfigurable, and Smart. *Adv. Funct. Mater.* **2018**, *28* (25), 1707228.

(4) Jang, B.; Hong, A.; Kang, H. E.; Alcantara, C.; Charreyron, S.; Mushtaq, F.; Pellicer, E.; Büchel, R.; Sort, J.; Lee, S. S.; Nelson, B. J.; Pané, S. Multiwavelength Light-Responsive Au/B-TiO $_2$ Janus Micromotors. *ACS Nano* **2017**, *11* (6), 6146–6154.

(5) Sridhar, V.; Park, B.-W.; Guo, S.; van Aken, P. A.; Sitti, M. Multiwavelength-Steerable Visible-Light-Driven Magnetic CoO–TiO $_2$ Microswimmers. *ACS Appl. Mater. Interfaces* **2020**, *12* (21), 24149–24155.

(6) Zhou, D.; Li, Y. C.; Xu, P.; Ren, L.; Zhang, G.; Mallouk, T. E.; Li, L. Visible-Light Driven Si–Au Micromotors in Water and Organic Solvents. *Nanoscale* **2017**, *9* (32), 11434–11438.

(7) Zheng, J.; Wang, J.; Xiong, Z.; Wan, Z.; Zhan, X.; Yang, S.; Chen, J.; Dai, J.; Tang, J. Full Spectrum Tunable Visible-Light-Driven Alloy Nanomotor. *Adv. Funct. Mater.* **2019**, 1901768.

(8) Chen, C.; Tang, S.; Teymourian, H.; Karshalev, E.; Zhang, F.; Li, J.; Mou, F.; Liang, Y.; Guan, J.; Wang, J. Chemical/Light-Powered Hybrid Micromotors with "On-the-Fly" Optical Brakes. *Angew. Chem., Int. Ed.* **2018**, *57* (27), 8110–8114.

https://doi.org/10.1021/acsanm.2c03560
ACS Appl. Nano Mater. XXXX, XXX, XXX–XXX

(9) María Hormigos, R.; Jurado Sánchez, B.; Escarpa, A. Multi-Light-Responsive Quantum Dot Sensitized Hybrid Micromotors with Dual-Mode Propulsion. *Angew. Chem., Int. Ed.* **2019**, *58* (10), 3128−3132.
(10) Zheng, J.; Dai, B.; Wang, J.; Xiong, Z.; Yang, Y.; Liu, J.; Zhan, X.; Wan, Z.; Tang, J. Orthogonal Navigation of Multiple Visible-Light-Driven Artificial Microswimmers. *Nat. Commun.* **2017**, *8* (1), 1438.
(11) Wang, J.; Xiong, Z.; Zhan, X.; Dai, B.; Zheng, J.; Liu, J.; Tang, J. A Silicon Nanowire as a Spectrally Tunable Light-Driven Nanomotor. *Adv. Mater.* **2017**, *29* (30), 1701451.
(12) Zhan, X.; Zheng, J.; Zhao, Y.; Zhu, B.; Cheng, R.; Wang, J.; Liu, J.; Tang, J.; Tang, J. From Strong Dichroic Nanomotor to Polarotactic Microswimmer. *Adv. Mater.* **2019**, *31* (48), 1903329.
(13) Chen, C.; Mou, F.; Xu, L.; Wang, S.; Guan, J.; Feng, Z.; Wang, Q.; Kong, L.; Li, W.; Wang, J.; Zhang, Q. Light-Steered Isotropic Semiconductor Micromotors. *Adv. Mater.* **2017**, *29* (3), 1603374.
(14) Chen, X.; Zhou, C.; Peng, Y.; Wang, Q.; Wang, W. Temporal Light Modulation of Photochemically Active, Oscillating Micromotors: Dark Pulses, Mode Switching, and Controlled Clustering. *ACS Appl. Mater. Interfaces* **2020**, *12* (10), 11843−11851.
(15) Sridhar, V.; Podjaski, F.; Alapan, Y.; Kröger, J.; Grunenberg, L.; Kishore, V.; Lotsch, B. V.; Sitti, M. Light-Driven Carbon Nitride Microswimmers with Propulsion in Biological and Ionic Media and Responsive on-Demand Drug Delivery. *Sci. Robot.* **2022**, *7* (62), eabm1421.
(16) Zhou, D.; Ren, L.; Li, Y. C.; Xu, P.; Gao, Y.; Zhang, G.; Wang, W.; Mallouk, T. E.; Li, L. Visible Light-Driven, Magnetically Steerable Gold/Iron Oxide Nanomotors. *Chem. Commun.* **2017**, *53* (83), 11465−11468.
(17) Zhou, D.; Li, Y. C.; Xu, P.; McCool, N. S.; Li, L.; Wang, W.; Mallouk, T. E. Visible-Light Controlled Catalytic Cu_2O−Au Micromotors. *Nanoscale* **2017**, *9* (1), 75−78.
(18) Xu, L.; Mou, F.; Gong, H.; Luo, M.; Guan, J. Light-Driven Micro/Nanomotors: From Fundamentals to Applications. *Chem. Soc. Rev.*.**2017**
(19) Villa, K.; Novotný, F.; Zelenka, J.; Browne, M. P.; Ruml, T.; Pumera, M. Visible-Light-Driven Single-Component $BiVO_4$ Micromotors with the Autonomous Ability for Capturing Microorganisms. *ACS Nano* **2019**, *13* (7), 8135−8145.
(20) Mou, F.; Kong, L.; Chen, C.; Chen, Z.; Xu, L.; Guan, J. Light-Controlled Propulsion, Aggregation and Separation of Water-Fuelled TiO_2/Pt Janus Submicromotors and Their "on-the-Fly" Photocatalytic Activities. *Nanoscale* **2016**, *8* (9), 4976−4983.
(21) Bialké, J.; Speck, T.; Löwen, H. Active Colloidal Suspensions: Clustering and Phase Behavior. *J. Non-Cryst. Solids* **2015**, *407*, 367−375.
(22) Wang, W.; Duan, W.; Sen, A.; Mallouk, T. E. Catalytically Powered Dynamic Assembly of Rod-Shaped Nanomotors and Passive Tracer Particles. *Proc. Natl. Acad. Sci. U.S.A.* **2013**, *110* (44), 17744−17749.
(23) Zöttl, A.; Stark, H. Emergent Behavior in Active Colloids. *J. Phys.: Condens. Matter* **2016**, *28* (25), 253001.
(24) Arzenšek, D. *Dynamic Light Scattering and Application to Proteins in Solutions*. Seminar, Department of Physics, University of Ljubljana, Ljubljana, Slovenia; 2010; pp 1−18.
(25) Abe, Y.; Kato, K.; Kawamura, M.; Sasaki, K. Rhodium and Rhodium Oxide Thin Films Characterized by XPS. *Surface Science Spectra* **2001**, *8* (2), 117−125.
(26) Koffyberg, F. P. Optical Bandgaps and Electron Affinities of Semiconducting Rh2O3(I) and Rh2O3(III). *J. Phys. Chem. Solids* **1992**, *53* (10), 1285−1288.
(27) Wang, Y.; Hernandez, R. M.; Bartlett, D. J.; Bingham, J. M.; Kline, T. R.; Sen, A.; Mallouk, T. E. Bipolar Electrochemical Mechanism for the Propulsion of Catalytic Nanomotors in Hydrogen Peroxide Solutions. *Langmuir* **2006**, *22* (25), 10451−10456.
(28) Paxton, W. F.; Kistler, K. C.; Olmeda, C. C.; Sen, A.; St. Angelo, S. K.; Cao, Y.; Mallouk, T. E.; Lammert, P. E.; Crespi, V. H. Catalytic Nanomotors: Autonomous Movement of Striped Nanorods. *J. Am. Chem. Soc.* **2004**, *126* (41), 13424−13431.
(29) Moran, J. L.; Posner, J. D. Role of Solution Conductivity in Reaction Induced Charge Auto-Electrophoresis. *Phys. Fluids* **2014**, *26* (4), No. 042001.
(30) Bär, M.; Großmann, R.; Heidenreich, S.; Peruani, F. Self-Propelled Rods: Insights and Perspectives for Active Matter. *Annu. Rev. Condens. Matter Phys.* **2020**, *11* (1), 441−466.

https://doi.org/10.1021/acsanm.2c03560
ACS Appl. Nano Mater. XXXX, XXX, XXX−XXX